International Journal of Rock Mechanics & Mining Sciences 47 (2010) 1289–1303

Contents lists available at ScienceDirect

International Journal of Rock Mechanics & Mining Sciences

journal homepage: www.elsevier.com/locate/ijrmms

Stability of shallow karstic caverns in blocky rock masses

Yossef H. Hatzor*, Ilia Wainshtein, Dagan Bakun Mazor

Department of Geological and Environmental Sciences, Ben-Gurion University of the Negev, Beer-Sheva 84105, Israel

ARTICLE INFO

Article history:
Received 26 October 2009
Received in revised form
8 September 2010
Accepted 10 September 2010
Available online 27 October 2010

Keywords:
Karst
Caves
Underground openings
Mining
Discrete element modeling
Blocky rock masses
DDA

ABSTRACT

The limiting relationship is explored between underground opening span and required cover height for stability in blocky rock masses characterized by a network of horizontal bedding planes and vertical joints. Understanding this relationship is crucial for the design of mining excavations in karstic terrain as typically encountered in carbonate rock masses. We perform numerical analysis of multiple roof spans vs. cover height geometries using the DDA method to obtain the boundary curve between stable and unstable opening geometries. Our results indicate that for cavern spans of up to 18 m a low cover height vs. opening span ratio of $h/B=0.33$ is sufficient for stability. For spans greater than 18 m the demand for cover height rapidly increases and it appears to stabilize at $h/B=1.0$ for $B=26$ m and above.

To validate our numerical analysis results, a unique case study is analyzed wherein a 40 m span karstic cavern, the Ayalon cave, has been preserved below an active open pit mine in central Israel with cover height of only 30 m, thus rendering the cave marginally stable according to our model prediction. Indeed there is ample evidence of partial collapse of the roof in the cave. The predictive capability of our model is further confirmed using two additional case studies in blocky rock masses, each of which possesses very different mechanical parameters such as intact rock strength, density, and deformability, suggesting that our model predictions remain valid as long the rock mass maintains a "blocky" structural configuration.

1. Introduction

The collapse of underground karst caverns due to excessive spans or insufficient rock cover is a major geological hazard in rock masses that are prone to the risk of sinkhole development [1–8]; accordingly, much research has been conducted recently on the detection of karstic caverns at depth using different geophysical methods [9–12] with various levels of success. Analytical solutions for the stability of shallow underground caverns in blocky rock masses are rarely used because of the inherently discontinuous nature of the problem; instead, numerical approaches such as the finite element [13], discrete element [14], or hybrid [15] methods of analysis are typically employed.

From our experience with bedded and fractured rock masses we find that the following rock mechanics factors control the stability of shallow karst caverns against structural collapse, listed below in order of descending importance: (1) height of rock cover; (2) span of the opening; (3) intensity of jointing characterized by the number of principal joint sets, mean spacing, and mean persistence discontinuities; (4) orientation of discontinuities; (5) shear strength of discontinuities; (6) strength of intact rock; (7) ground water conditions.

The main challenge in performing rock engineering works in ground susceptible to sinkhole collapse is the lack of basic guidelines for prediction of shallow cavern stability for given span width and cover height. For deep excavations, with rock cover much greater than the excavation span, preliminary assessment of the height of the loosened zone above the immediate roof of the opening may be obtained on the basis of the empirical Terzaghi's rock load classification [16]. We find Terzaghi's predictions valid when compared with field observations [e.g. [17,18]] and numerical analyses [e.g. [19,20]]. Geotechnical stability problems ensue when the cover height is nearly as large as the excavation span, or even smaller. In such cases the karstic caverns may be said to be of precarious stability: they may hold for many years [e.g. [18]] or collapse without preliminary warning with the failure zone breaking the ground surface [e.g. [10]].

Consider open pit mining operations in a ground prone to sinkhole collapse. Assuming the existing karst caverns are explored before mining operations begin, either by employing geophysical methods or simply by drilling exploration boreholes, the minimum required rock cover (h) for a given cavern span (B) after the excess over burden is removed must be known in advance for safe mining operations (see Fig. 1). This relationship will also help determine three economically significant mining parameters: (1) the maximum safe permanent bench height (H), (2) the minimum required diagonal distance between exploration boreholes (d), and (3) the minimum required exploration drilling depth (D) (see Fig. 1).

We begin with numerical analyses of cavern span width vs. cover height in synthetically generated blocky rock masses to obtain, semi-empirically, the limiting relationship between those two parameters. We then proceed with a case study that supports our numerical results and shows their applicability in real mining.

* Corresponding author. Tel.: 972 8 6472621; fax: 972 8 6472997.
E-mail address: hatzor@bgu.ac.il (Y.H. Hatzor).

1365-1609/$ - see front matter © 2010 Elsevier Ltd. All rights reserved.
doi:10.1016/j.ijrmms.2010.09.014

2. Numerical approach

2.1. Geometry of the modeled caverns

To determine the critical relationship between opening span and minimum required rock cover for stability we model the deformation of theoretical caverns with a horse-shoe cross-sectional geometry and the following variable parameters (Fig. 2): cavern span (B), height ($H=0.5B$), roof curvature ($c=0.5H$), and rock cover after excess overburden is removed ($=h$). The modeled domain is extended laterally to its boundaries by a distance of $b=2B$. The infinite lateral continuity of the rock mass beyond the analyzed domain is modeled by fixed boundaries as shown in Fig. 2. The ground surface is modeled as a horizontal plain. A total of nineteen cavern geometries of varied spans and rock covers are modeled with details as listed in Table 1.

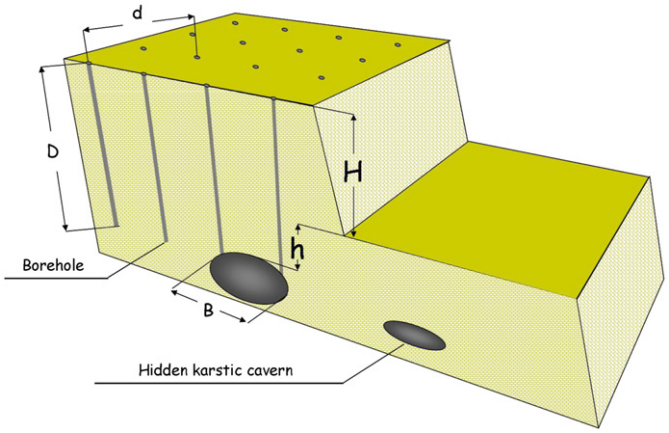

Fig. 1. Schematic illustration of a possible exploration procedure to detect hidden karstic caverns below the excavated bench. D=depth of exploratory drill holes, d=diagonal distance between boreholes, H=designed bench height, h=depth of rock cover after excess overburden is removed, and B=hidden karstic cavern span.

2.2. Statistical generation of rock structure

The modeled structure is typical for sedimentary rock masses prone to karst formation, and is generated here synthetically with one set of horizontal bedding planes of infinite persistence, transected by two orthogonal and vertically dipping joint sets of limited extent. Synthetic joint trace generation is performed with the DL code of the 2D-DDA software package, a statistical line generation code that is based essentially on the unrolling algorithm of Shi and Goodman [21]. The mean spacing, bridge length, and degree of randomness used for statistical joint trace generation are listed in Table 2; for precise definition of terminologies see [21]. The attitude, trace length, and bridge length of each joint set are determined from statistical analyses of scan lines and photographs performed in connection with the case study described later in this

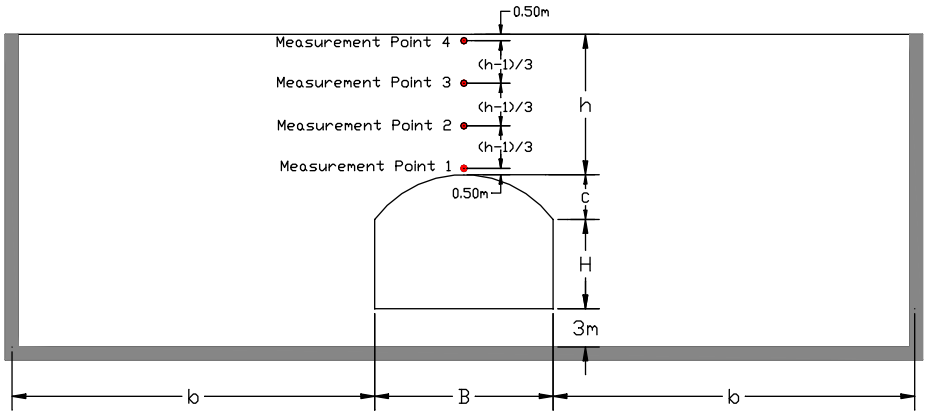

Fig. 2. Definition of geometrical terms for numerical modeling of hidden karstic caverns, measurement point location for numerical analysis output is indicated as well.

Table 1
Matrix of modeled cavern geometries and resulting stability (columns in bold).

Model number	Cavern span B (m)	Boundary distance b (m)	Cavern height H (m)	Roof curvature c (m)	Cover height h (m)	Surface settlement s (m)	Settlement ratio s/h	Obtained structural configuration
1	10	20	5	2.5	6	**−0.0313**	**0.0052**	**Stable**
2	14	28	7	3.5	6	**−0.0537**	**0.0089**	**Stable**
3	14	28	7	3.5	11	**−0.0382**	**0.0035**	**Stable**
4	17	34	8.5	4.25	6	**−0.1164**	**0.0194**	**Stable**
5	20	40	10	5	6	**−2.1122**	**0.3520**	**Unstable**
6	20	40	10	5	10	**−0.2065**	**0.0207**	**Stable**
7	20	40	10	5	14	**−0.2871**	**0.0205**	**Stable**
8	40	80	20	10	15	**−3.5729**	**0.2382**	**Unstable**
9	40	80	20	10	20	**−1.9855**	**0.0993**	**Unstable**
10	40	80	20	10	25	**−1.9004**	**0.0760**	**Unstable**
11	30	60	15	7.5	15	**−2.2442**	**0.1496**	**Unstable**
12	30	60	15	7.5	22	**−2.4329**	**0.1106**	**Unstable**
13	30	60	15	7.5	30	**−0.5349**	**0.0178**	**Stable**
14	25	50	12.5	6.25	12.5	**−2.4728**	**0.1978**	**Unstable**
15	25	50	12.5	6.25	25	**−1.0131**	**0.0405**	**Marginal**
16	25	50	12.5	6.25	19	**−0.4607**	**0.0242**	**Marginal**
17	25	50	12.5	6.25	30	**−0.2970**	**0.0099**	**Stable**
18	22	44	11	5.5	11	**−4.2015**	**0.3820**	**Unstable**
19	22	44	11	5.5	22	**−0.2425**	**0.0110**	**Stable**

paper. Once all lines are generated the DDA block cutting algorithm is applied using the DC code of the DDA package. The selected cross-section direction for the statistically generated 2D block system is the one in which the total removable keyblock area in the roof is maximum (for details see for example [22]), found to be striking to azimuth 142 for the joint orientation data shown in Table 2.

2.3. Forward modeling with DDA

Forward modeling of discontinuous deformation is performed with the DF code of 2D-DDA software package. The discontinuous deformation analysis (DDA) is an implicit discrete element method proposed originally by Shi [23] to provide a tool useful for investigating the kinematics of blocky rock masses. DDA models a discontinuous material as a system of individually deformable blocks that move independently with minimal amount of interpenetration. The formulation is based on dynamic equilibrium that considers the kinematics of individual blocks as well as friction along block interfaces. The displacement and deformation of the discrete blocks are the result of the accumulation of small time steps. The equilibrium equations are derived by minimizing the total potential energy of the block system with respect to the displacement at block center. In this study, we use the original two dimensional version of DDA in which each block i in the general block system has six degrees of freedom, and the resulting displacement components (u, v) of an arbitrary point (x, y) in X and Y directions are derived using a first order approximation. The algebraic equation for the increase in displacement is solved for each time increment by substituting the appropriate terms for acceleration and velocity provided by a time integration formulation similar to Newmark direct integration method with parameters $\beta=0.5$ and $\gamma=1.0$, into the general equation of motion [24,25]. The result is a system of equations for solving the dynamic problem which is, after collecting terms on both sides, typically expressed as $\hat{K}D=\hat{F}$, where K_{ij} is a 6×6 coefficient sub-matrix, D_i is a 6×1 deformation matrix of block i, and F_i is a 6×1 loading matrix of block i. Sub-matrices $[K_{ii}]$ depend on the material properties of block i and sub-matrices $[K_{ij}]$ are defined by the contacts between blocks i and j. A good review of DDA formulation is provided by Jing [26]. The validity and accuracy of DDA has been studied extensively over the past decade and a comprehensive review is presented in [27]. Three user-specified, numeric control parameters are required in DDA: the normal contact spring stiffness ($g0$), the time step size ($g1$), and the assumed maximum displacement per time step ratio ($g2$). The possible range for these control parameters in relation to the size of the modeled domain and the mean length of blocks in the mesh is discussed in [23]; optimal values for problems involving underground excavations in highly discontinuous rock masses are suggested in [20].

The modeled deformation is computed for gravitation loading under dynamic conditions, namely every block in the modeled domain inherits the terminal velocity from the previous time step (K01=1.0 in DDA terminology). Following intensive research and validation studies for dynamic DDA using field studies [28,29] and shaking table experiments [30] it seems that for problems involving the dynamic interaction of multiple blocks a kinetic damping of 1% would result in the greatest accuracy. With 1% kinetic damping every block in the modeled domain inherits 99% of its terminal velocity from the previous time step. The necessity to introduce some amount of damping into dynamic DDA computations is probably because the theory of DDA ignores inelastic and irreversible deformation processes that must be active in the physical world, such as for example breakage at block corners, energy dissipation due to heat generation during slip, etc.

Table 2
Geometrical input parameters for block system generation with DL code.

Joint set	Dip/ direction	Trace length	Mean spacing (m)	Degree of randomness	Rock bridge length (m)
1	0/0	∞	0.70	1.0	0
2	88/182	5 m	0.96	0.5	2.5
3	88/102	5 m	0.78	0.5	2.5

Table 3
Mechanical and numerical input parameters for forward modeling with DF code.

Unit weight	22.54 kN/m^3
Young's modulus	15.32 GPa
Poisson's ratio	0.21
Friction angle of discontinuities	30°
Cohesion of discontinuities	0 MPa
Tensile strength of discontinuities	0 MPa
Normal spring stiffness	500 MN/m
Shear spring stiffness	250 MN/m
Initial time step size	0.0005 s
Kinetic damping	1%

Table 4
Numerical characteristics of each computed model with 2D-DDA (single Pentium IV, 3 GHz processor).

Model	Total number of blocks	Total number of time steps	Maximum allowable displacement per time step (cm)	Average number of iterations per time step	Real time computed (s)	CPU time (h)
1	871	20,000	0.413	1.479	10.00	1.83
2	1325	20,000	0.488	1.862	10.00	2.36
3	1780	20,000	0.613	2.338	10.00	3.66
4	2123	20,000	0.544	2.191	10.00	6.17
5	2221	20,000	0.600	2.793	9.97	7.65
6	2715	20,000	0.700	2.375	9.96	8.60
7	3197	20,000	0.800	2.741	9.92	10.92
8	8638	40,000	1.200	4.317	18.50	89.33
9	9948	40,000	1.325	4.821	16.89	130.00
10	11104	40,000	1.450	5.067	16.15	138.00
11	5720	30,000	1.013	3.486	14.55	48.00
12	6947	30,000	1.188	4.051	13.93	50.10
13	8157	35,000	1.388	4.322	15.24	78.20
14	4287	30,000	0.856	3.134	14.85	25.58
15	5925	40,000	1.169	3.279	14.43	35.90
16	5086	30,000	1.019	3.608	13.96	37.10
17	6591	30,000	1.294	3.714	13.75	46.92
18	3240	30,000	0.763	3.007	14.90	16.88
19	4683	30,000	1.038	3.098	14.29	27.21

2.4. Incorporation CAD into DDA mesh generation scheme

The DL and DC codes of the 2D-DDA software package are the preprocessors that generate a blocky rock mass domain for forward analysis of deformation. The input text files for these preprocessors have a well defined structure, are usually written manually and typically include the following data sets: (1) boundary geometry of domain, (2) statistically generated or manually input joint sets and their assigned material properties, (3) assigned material properties for intact rock blocks, (4) location and geometry of underground openings, (5) location of measurement, fixed and loading points

The compilation of such input data files, especially for very complex problem geometries, may be very complicated and time consuming. In order to facilitate this process we employ here CAD software. The geometrical nature of the problem and the well defined input file structure are the main motivation to do so.

A typical CAD drawing is usually composed of layers. The main concept of a layer in the CAD system is to categorize drawing

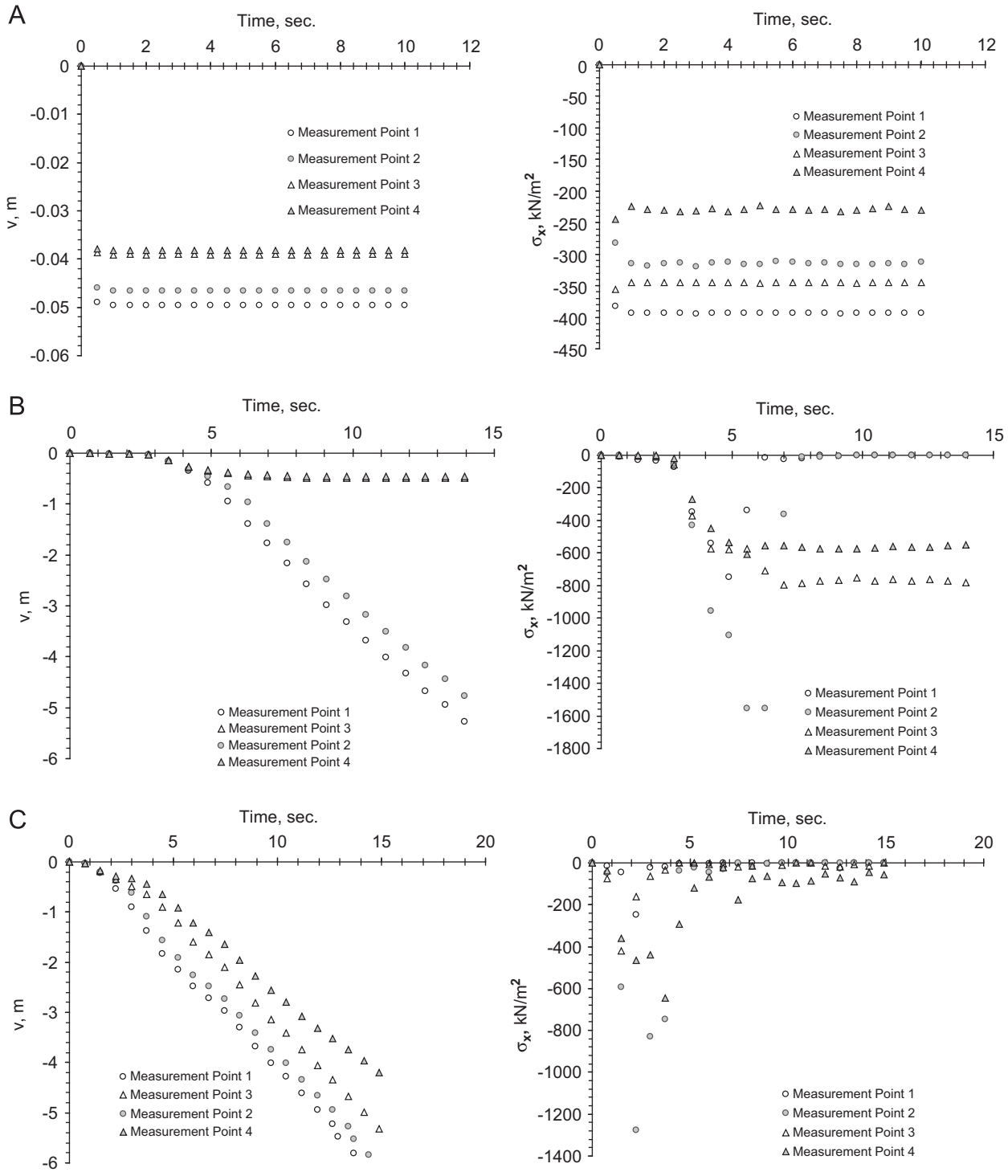

Fig. 3. Definition of obtained structural configurations with DDA using representative outputs recorded at the four measurement points in the roof; for measurement point location see Fig. 2: (A) stable structure (model 3), (B) marginally stable structure (Model 16), (C) unstable structure (Model 18).

elements into sets. For example, layers of architectural objects, construction elements, electrical wires, etc., can be a part of a typical CAD drawing. In the same manner layers for different DDA data sets can be created. For example, a measurement point on such a drawing may be represented by a circle drawn in layer "ms_point" and its center will be located at a desirable position within the domain. The same idea could be applied to the other DDA data sets. CAD programs usually allow retrieving the drawing objects characteristics, such as layer name, line ends or circle center coordinates, as a log (text) file. The data from this log file may be filtered, sorted and converted easily to DL or DC input file format through some simple programming.

3. Results of numerical analysis

In the nineteen cavern geometries that are modeled the spans (B) range from 10 to 40 m and the cover heights (h) range from 6 to 30 m (see Table 1). The resulting rock mass structures consist of a large number of discrete elements representing individual blocks, from as low as 871 blocks in the smallest model (1) to as many as 11,104 blocks in the largest model (10); see Table 4.

Four equally spaced measurement points are positioned at the center line of the roof as shown in Fig. 2. During the progress of the numerical computation the following output parameters are stored in each measurement point: (u, v, σ_x, σ_y, τ_{xy}), where u and v are displacements in x and y directions, respectively, σ_x, σ_y, and τ_{xy} are normal and shear stresses. The mechanical and numerical control input parameters used for the simulations are listed in Table 3.

Numerical computations are performed on a standard PC with a single Pentium IV, 3 GHz processor. For each computed model the total number of generated blocks, the total number of time steps, the maximum allowable displacement per time step, the average number of iterations per time step, the real time computed, and the total CPU time required to complete the computational task, are listed in Table 4. The total duration of the simulation (as expressed by the user specified number of time steps and more accurately by the total real time actually computed at the end of the simulation) is increased with increase in number of elements in the modeled block systems, so as to allow for gravity to take effect in all the blocks in the mesh before actual deformation due to the underground opening begins.

Inspection of Table 4 reveals that the computation of models with a total number of blocks greater than several thousands is very time consuming with a single 3 GHz processor, for example a CPU time of 138 h is required for the largest computer model (10). The obtained average number of iterations per time step, a measure of the efficiency of the numerical convergence and the adequacy of the selected numerical control parameters, is very reasonable.

3.1. Definition of structural configurations

The results of the numerical simulations are discussed in terms of three structural configurations that are obtained at the end of the analysis using the recorded and stored values of vertical displacement (v) and horizontal stress (σ_x) at the four measurement points as follows: (1) stable, (2) marginally stable, and (3) unstable structural configurations.

A stable structural configuration is obtained when, following the immediate elastic response of the system due to the opening, the change in vertical displacement over time is zero (see left panel in Fig. 3A for example), namely $\dot{v} = dv/dt = 0$. A zero vertical

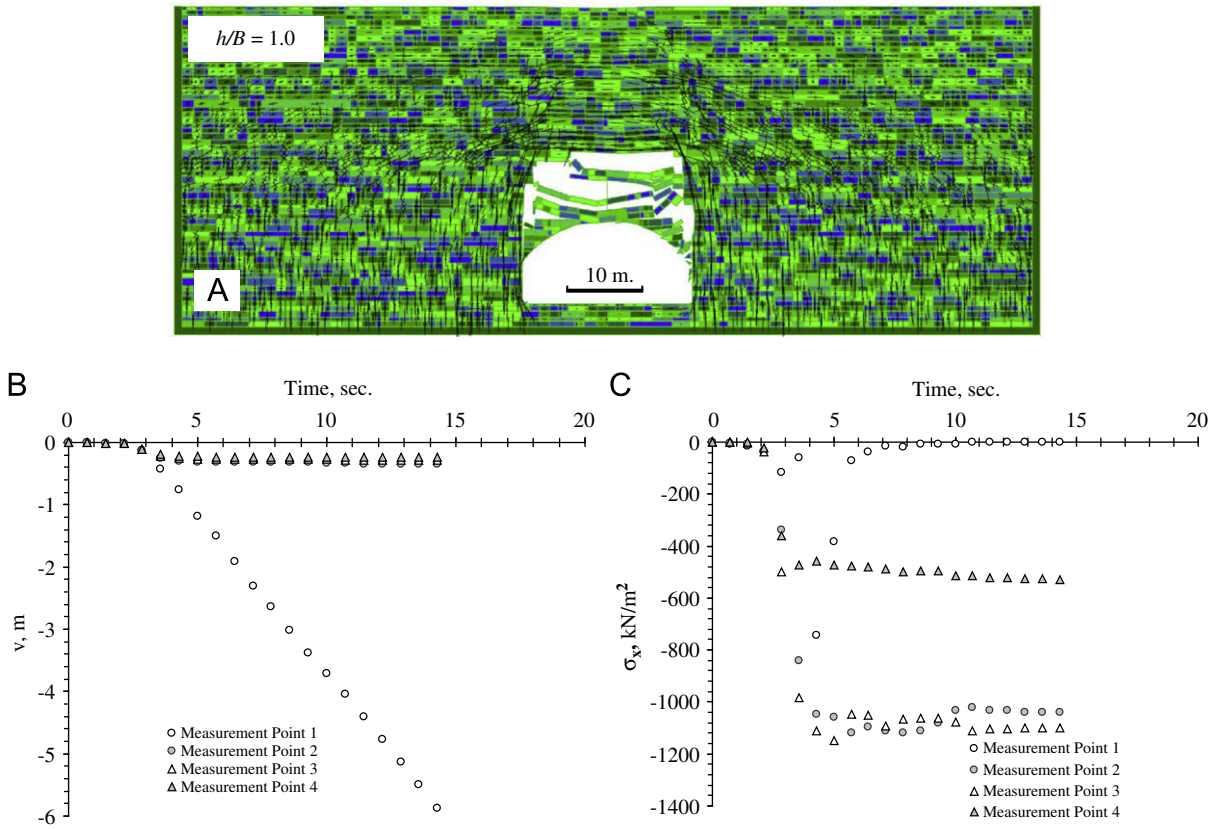

Fig. 4. Extension of the definition of stable structural configuration to cases where only the immediate roof layers collapsed while the remaining roof structure attained stability: (A) graphical output of a forward DDA computation for a typical model in this category (Model 19, B=22) after 15 s or gravitational loading, principle stress trajectories show the height and extent of the compressive arching stresses in the roof, (B) vertical displacement, and (C) horizontal stress vs. time; for measurement point location, see Fig. 2).

displacement rate at the centerline of the roof suggests that effective arching stresses have developed in the deformed roof, thus arresting any further downward displacement of the roof strata after the immediate elastic response stage. Stable arching is further indicated by the development of homogeneous compressive horizontal stresses in all four measurement points in the roof during deformation (see right panel in Fig. 3A for example, where by convention compression is negative).

We extend the definition of stable structural configuration to those cases where the immediate roof collapses (measurement point 1) but the remaining three quarters of the roof (measurement points 2–3–4) remain static ($\dot{v}=0$) afterwards (see for example Fig. 4A). Because we are concerned here with the global stability of the entire structure, rock mass and cavern together, the loss of the immediate roof layers is considered a response to loosening below the compressive arch that is formed in the roof, and not an indication of global structural instability. Indeed, while measurement point 1 exhibits falling, the remaining measurement points exhibit stability ($\dot{v}=0$) following initial elastic response to the opening (Fig. 4B). This conclusion is supported by the recorded horizontal stress data (Fig. 4C). It is interesting to note that the horizontal stress history of measurement point 1 (Fig. 4C) suggests that a kind of a "three hinged beam" or "Voussoir" analogue [31,32] is formed at the immediate roof layer during the elastic response stage, as horizontal compressive stresses build up there to a rather high level of 700 kPa. With further deformation of the surrounding structure, however, the temporary three hinged beam mechanism collapses and the developed horizontal stresses drop to zero. In contrast, measurement points 2–3–4 exhibit stability ($\dot{v}=0$) with stable arching stresses of σ_x=1100, 1150, and 500 kPa, respectively.

Note that for the case of free falling blocks (e.g. measurement points 1 and 2 in Fig. 3B) the velocity of the falling blocks is apparently constant ($\dot{v}=c$), namely no acceleration under gravity is indicated in contrast to intuition for free falling bodies. This artifact is a result of the imposed 1% kinetic damping applied in all DF simulations.

Marginal structural configuration is defined here when in the process of arching the lower half of the roof (measurement points 1, 2) fails but the upper half of the roof (measurement points 3, 4) remains stable (see Fig. 3B). Using the deformation data recorded at the four measurement points in the roof this structural configuration is expressed by ongoing downward displacement of measurement points 1, 2 at a constant vertical displacement rate $\dot{v}$, whereas the upper measurement points (3, 4) exhibit stability ($\dot{v}=0$).

Unstable structural configuration is defined here when the entire roof collapses or when the three lower measurement points exhibit ongoing downward displacement. An example is shown in Fig. 3C demonstrating ongoing downward displacement of all four measurement points, none of which exhibits stability, as well as erratic horizontal stress history in all four measurement points that rapidly approaches zero. When such a scenario is developed the collapse of the karstic cavern underground will have a clear surface manifestation as it will break the ground.

3.2. Influence of roof span and cover height on stability

Underground caverns in blocky rock masses are expected to be less stable with increasing span per a given height of overburden. A typical rule of thumb in the mining and tunneling industries is that at least two tunnel diameters are required as cover height to ensure stability

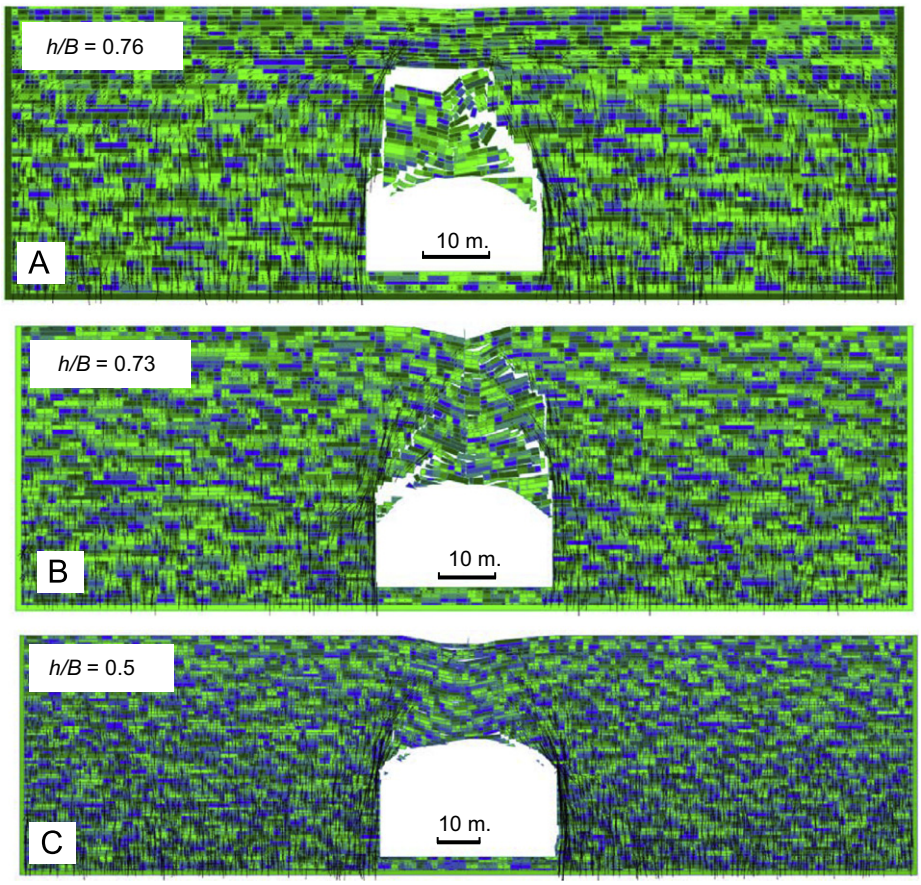

Fig. 5. Influence of roof span on cavern stability and rock mass deformation: (A) B=25 m, h=19 m (Model 16), (B) B=30 m, h=22 m (Model 12), and (C) B=40 m, h=20 m (Model 9).

in portal areas; for deeper section Terzaghi's rock load classification may be employed [16], predicting that for the blocky rock mass modeled here the loosened zone height is expected to be 0.5*B*.

To demonstrate the influence of cavern diameter, four representative cases for shallow caverns with overburden height of approximately $h=20$ m are shown in Figs. 4 and 5. In Fig. 4 the deformation of a cavern with h/B ratio of 1.0 is shown ($B=22$ m). While the immediate roof layer collapses following the opening as discussed in the previous section, the remaining roof strata remain completely intact, indicating stability. With increase in span to $B=25$ m ($h/B=0.76$) the opening becomes marginally stable (Fig. 5A), and completely unstable with the loosening zone breaking out to the ground surface when the span approaches 30 m ($h/B=0.73$, Fig. 5B), and 40 m ($h/B=0.5$, Fig. 5C).

The influence of cover height on cavern stability is studied in the same way, by selecting a fixed cavern span of $B=25$ m and analyzing the influence of cover height. Three representative simulations are shown in Fig. 6 starting with a deep cavern ($h/B=1.2$, Fig. 6A) that exhibits perfect stability, continuing to

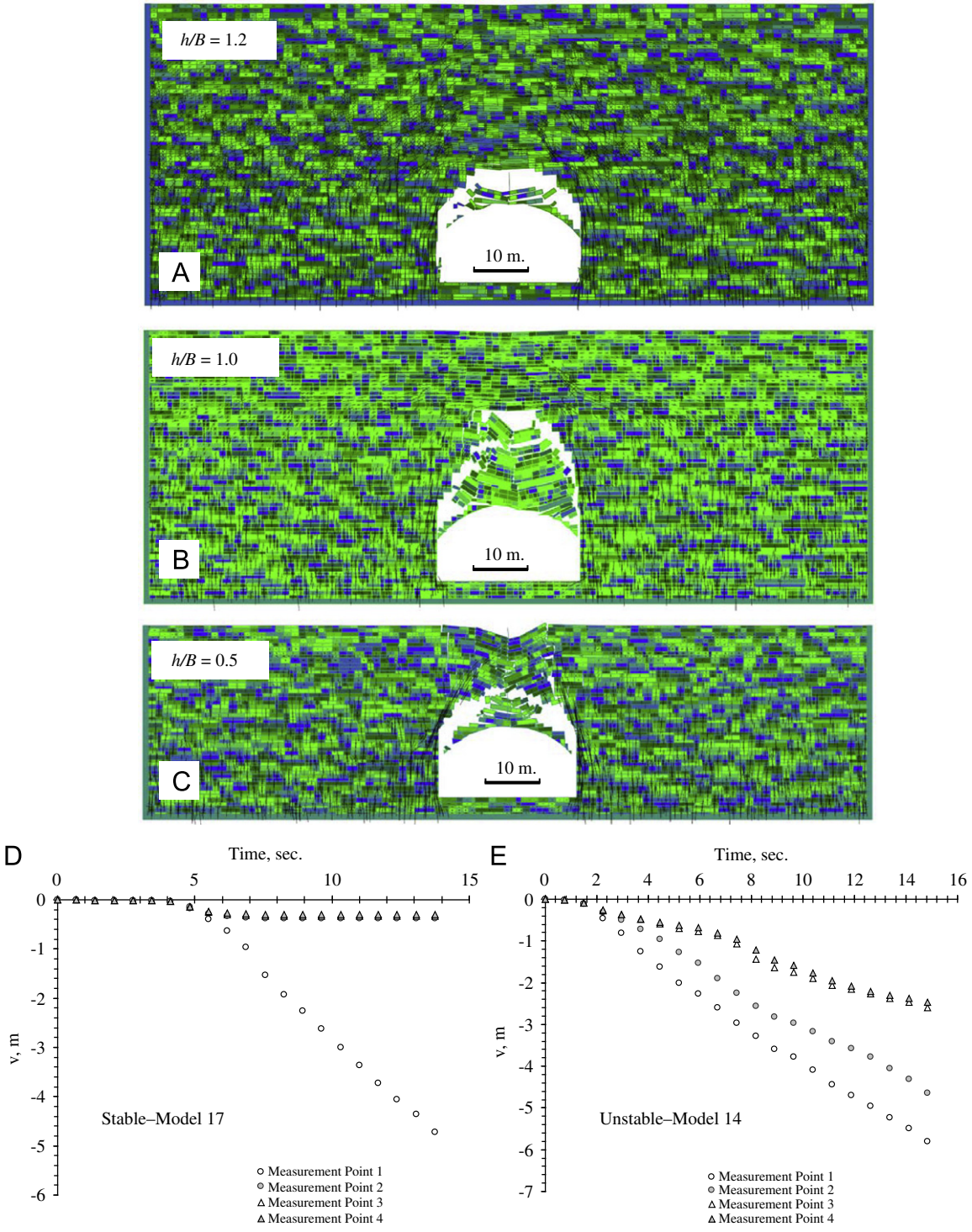

Fig. 6. Influence of cover height on cavern stability ($B=25$ m): (A) $h=30$ m (Model 17); (B) $h=25$ m (Model 15); (C) $h=12.5$ m (Model 14). Vertical roof deflection as measured in four measurement points for stable (D) and unstable (E) configurations.

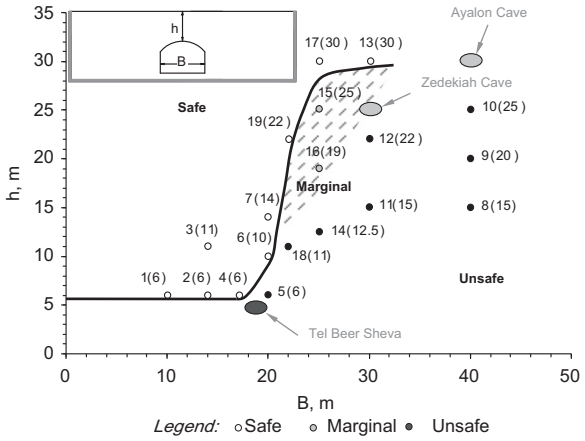

Fig. 7. Boundaries between safe, marginal, and unsafe geometries for shallow caverns in blocky rock masses. DDA model # above symbols, cover height in parenthesis.

decrease in the cover height of 25 m ($h/B=1.0$, Fig. 6B) where stability is obtained, down to cover height of 12.5 m only ($h/B=0.5$, Fig. 6C) where total collapse is indicated.

Our analysis clearly demonstrates that for shallow caverns in blocky rock masses the opening may become marginally stable when the cover height is smaller than the cavern span. Complete collapse may be anticipated when $h/B<0.75$.

Note that this numerical result renders Terzaghi's rock load prediction, typically considered to be overly conservative in the tunneling and mining industries, unconservative, as the height of the loosened zone found in our analysis is greater than $0.5B$ when $h/B<0.75$. Terzaghi's classification, however, was not intended for shallow openings and as mentioned in the introduction is often found valid in deeper excavations, as can also be appreciated by inspection of our Fig. 6A and B.

To refine the boundaries obtained by us numerically between safe, marginal, and unstable caverns we plot the results of all 19 DDA simulations in span width (B) vs. cover height (h) space. As can be seen in Fig. 8, the shape of the refined boundary between safe and unsafe

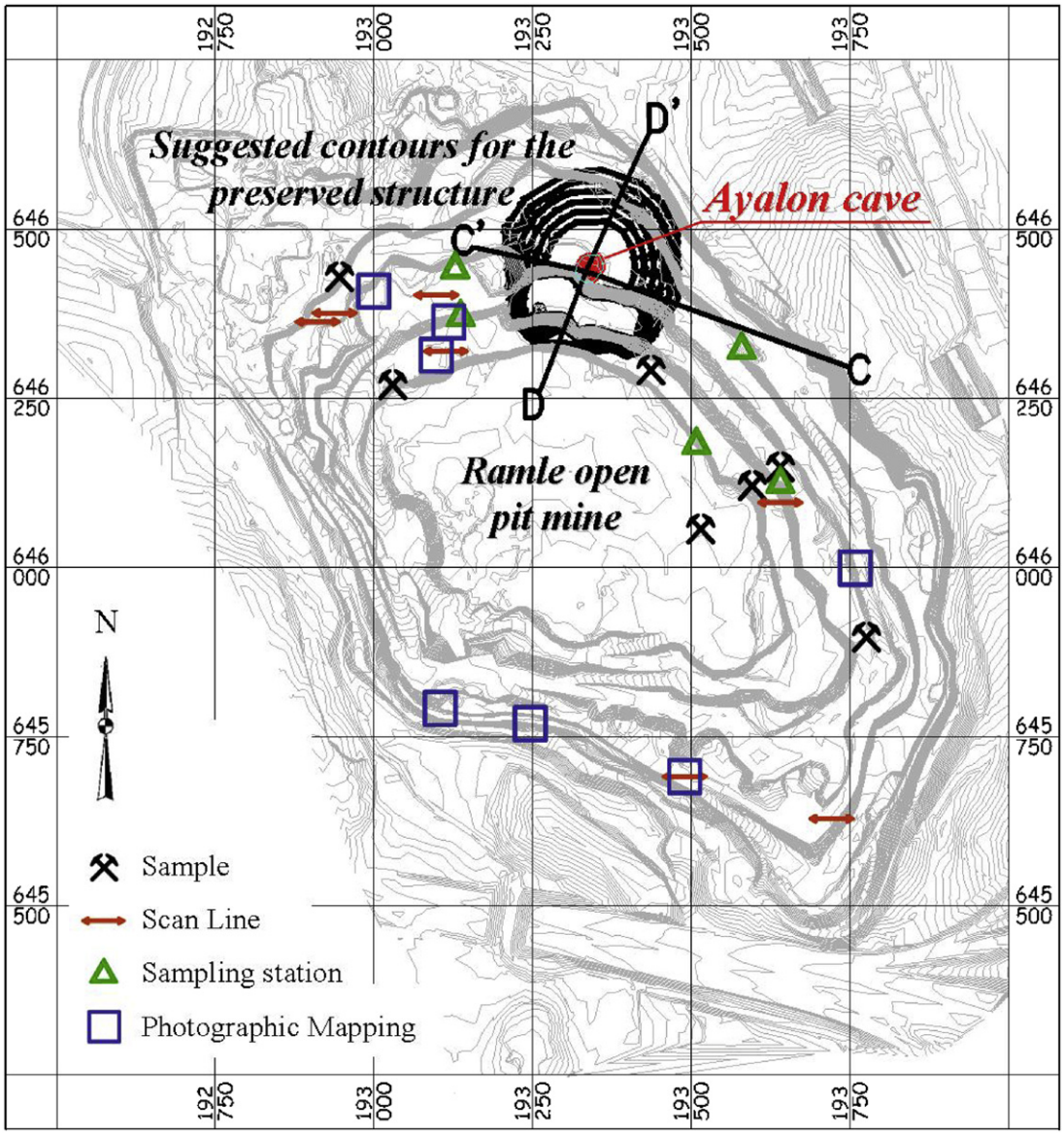

Fig. 8. Topographic contour map for Ramle open pit mine with projection of the Ayalon underground cavern (heavy contours in the north slope of the mine) and sampling sites for rock testing and joint survey.

geometries assumed an S shape, allowing for lower h/B ratios in very shallow caverns ($h=6$ m) up to a span of $B=18$ m. For greater spans the demand for cover height increases very rapidly from $h/B=0.33$ for $B=18$ m to $h/B=1.0$ for $B=26$ m. Beyond $B=26$ m, the demand for cover/span ratio seems to remain constant at $h/B=1.0$.

Finally, to provide a quantitative measure for our results we suggest a "settlement ratio" defined as the ratio between total surface settlement (s) and cover height (h) above the opening. For each one of the nineteen models the total surface settlement computed numerically after the block system has stabilized is recorded from the vertical displacement component of the uppermost measurement point No. 4 (see Fig. 2). The s value thus obtained is normalized by the cover height in each model and the settlement ratio of s/h is thus obtained. Interestingly, a settlement ratio of $s/h=0.05$ is found to mark the boundary between stable and unstable configurations, with all unstable configurations exhibiting a settlement ratio greater than 0.05. The settlement ratios obtained for all models at the end of the computation are tabulated in Table 1.

4. Case study: the Ayalon cave

Below the Nesher limestone quarry, near the city of Ramle of central Israel, a very large hidden karstic cave was explored during routine mining operations in 2006 (see Fig. 8). With average span of 40 m and cover height of only 30 m the underground structure may be considered marginally stable considering the results of our numerical study discussed above (Fig. 7).

Since the cavern has been sealed off from the outside world for millions of years, a unique ecosystem developed in a disconnected groundwater pond inside the cavern (Fig. 9A), where eight ancient animal species that had never been recognized before by modern science were found. At 2.5 km long, the Ayalon cave is Israel's second largest known limestone cave. Four of the new species are water-dwelling crustaceans and four others are land-based invertebrates—creatures without spines. Also found in the cave were bacteria that serve as the basic food source in the self-contained community. As might be expected of species confined to a pitch-black cavern for millions of years, none of the newly discovered animals had eyes [33].

Following the discovery of the cave a comprehensive rescue and preservation effort has been embarked by Nesher Cement Industries Ltd. and Israel Ministry of Infrastructure to allow further scientific exploration of the species in the cave while ongoing mining operations continue in the mine above and around it. The rock engineering challenge is to determine the stability of the cavern after the mine layout would be modified by leaving a disconnected trapezoidal rock structure encompassing Ayalon cave in the middle of the mine, while mining operation continues around it.

4.1. Rock mass properties

The physical and mechanical properties of the rock in the mine were determined using comprehensive sampling in the field (sampling locations in Fig. 8), point load, Brazilian, and standard uniaxial compression tests (UCS) with electronic strain gages for elastic parameter determination. The rock mass consists the medium strength Bina limestone formation with mean UCS of 44 MPa, Young's modulus of 15 GPa, and Poisson's ratio of 0.21 (see Fig. 10A–D). The mean bulk density and the porosity exhibit a strong correlation with rock strength (Fig. 10E) with mean bulk density in natural water content conditions of 2087 kg/m^3.

The statistical parameters of the discontinuities were determined in several scan line surveys performed in the field, coupled with measurements performed directly on photographs in the case of inaccessible rock exposures in the mine. Three sets of principal

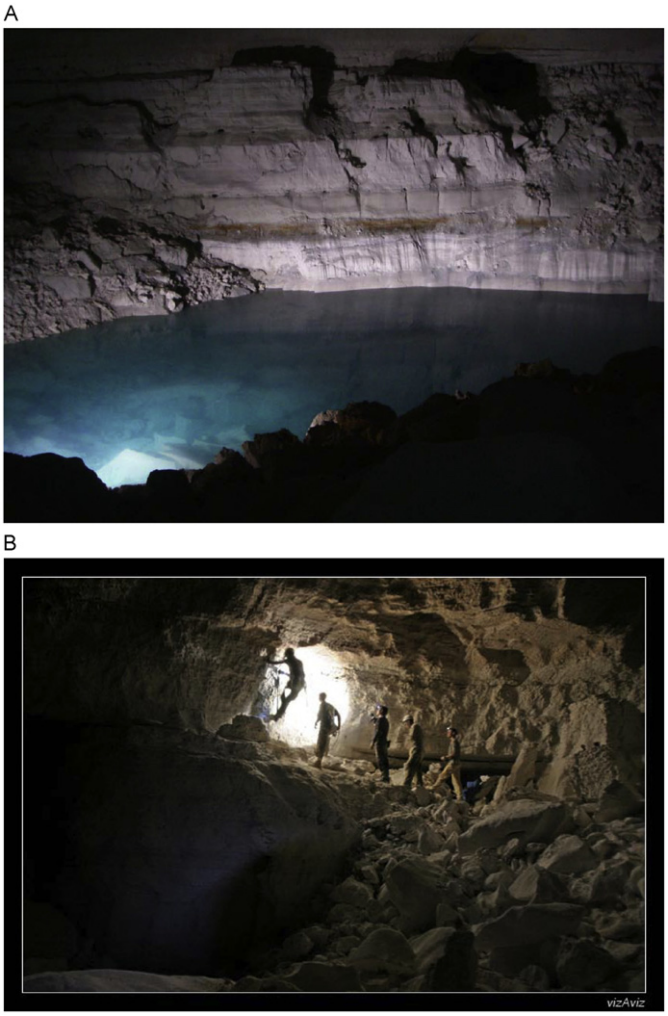

Fig. 9. (A) The disconnected ground water pond inside the karstic Ayalon cave where eight previously unrecognized species were classified and (B) inside view of the roof of Ayalon cave (photos courtesy of A. Frumkin).

discontinuities consists the rock mass structure: a set of horizontal bedding planes of infinite extent, and two sub-vertical and orthogonal joint sets (see Table 2). The orientation and spacing distribution of each individual joint set are shown graphically in Fig. 11.

Shear strength of discontinuities was determined in the lab using direct shear tests in the hydraulic, servo-controlled, direct shear system at Ben-Gurion University manufactured by TerraTek Systems (see Fig. 12A). The system shear box dimensions are 15 cm × 15 cm × 30 cm, normal and horizontal force capacities are 1000 and 300 kN, respectively, horizontal shear and vertical dilatational displacements are monitored with two and four LVDT's, respectively, each transducer with a range of 50 mm and 0.25% linearity full scale. Both normal and shear pistons are operated in closed loop servo control with two control modes: load and displacement. The results of three direct shear test segments each at a different normal stress level for a representative bedding plane surface are shown in Fig. 12B. Determination of the shear stiffness was performed from linear regression along the experimentally obtained linear elastic part of the shear stress–shear displacement curves for each segment (Fig. 12C). To study the residual shear strength of the bedding planes under a very low normal stress level several tilt tests of saw-cut surfaces were performed in additional to the servo controlled direct shear tests of naturally rough surfaces. The experimentally obtained peak

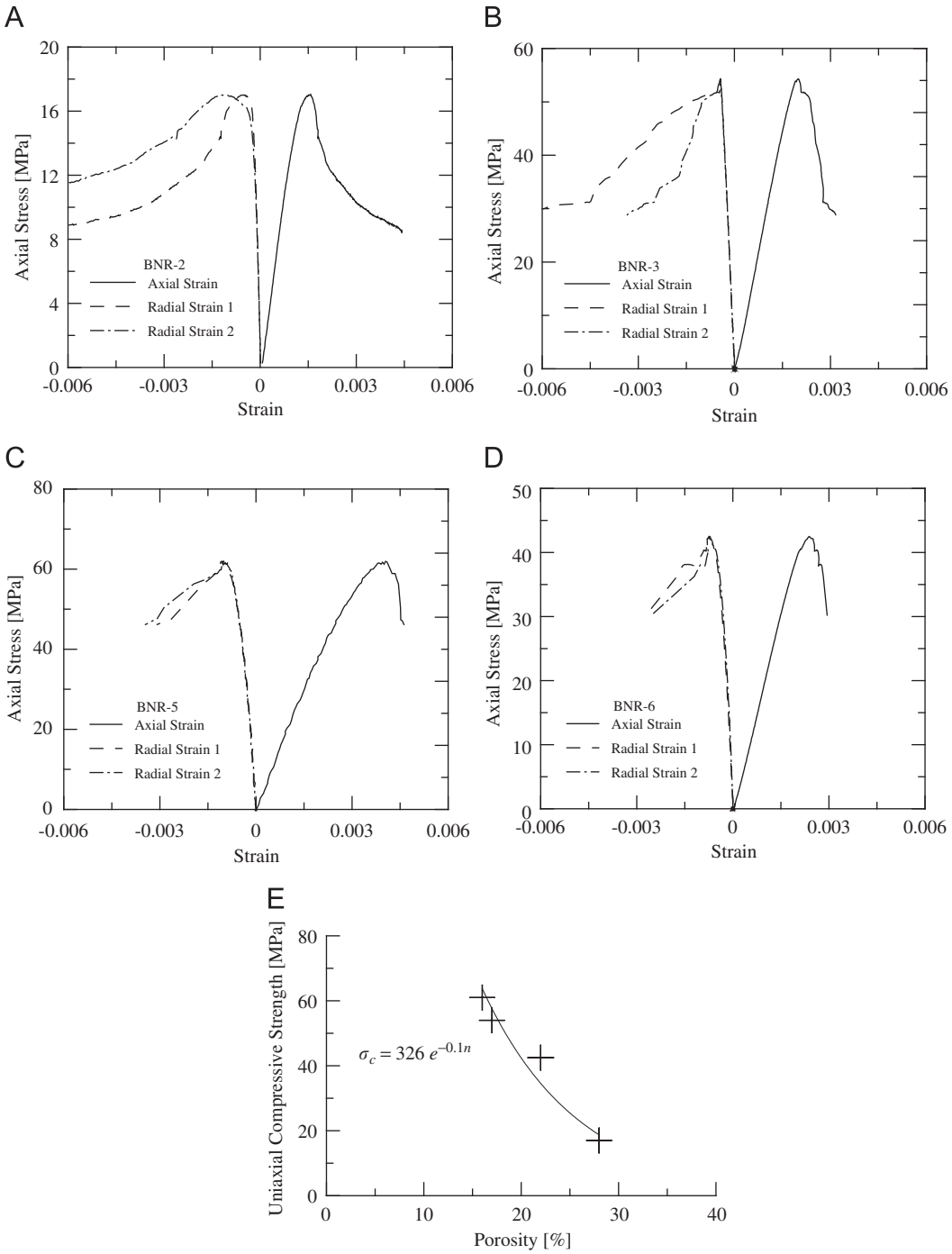

Fig. 10. (A–D) Four uniaxial compression test results for four representative Bina limestone samples from Ramle mine and (E) relationship between uniaxial compressive strength of Bina limestone and bulk porosity.

friction angle for rough surfaces is 42° and the residual friction angle obtained for saw cut surfaces is 24° only.

To confirm the experimental results obtained from a single direct shear test with three segments, the shear failure criterion of Barton [34]: $\tau = \sigma_n \tan[\mathrm{JRC}\log_{10}(\mathrm{JCS}/\sigma'_n) + \phi'_r]$ was computed based on twenty roughness profiles and 68 Schmidt hammer tests measured in the field. The resulting joint roughness coefficient (JRC) and joint compressive strength (JCS) values are 10.7 and 37 MPa, respectively, the latter is in good agreement with experimental results. With a residual friction angle of $\phi_r = 24°$ the dilation angle obtained by Barton's criterion, $\mathrm{JRC}\log_{10}(\mathrm{JCS}/\sigma'_n)$ for a normal stress level of $\sigma'_n = 1$ MPa is 16.7°, resulting in a peak friction angle of 40.7°, very close to the value obtained experimentally. For numerical modeling a value of 41° was selected due to the relatively low stress acting on both vertical and horizontal discontinuities in the field; all other input parameters are listed in Table 3.

4.2. Proposed preservation of Ayalon cave

To preserve the Ayalon cave for further scientific study of the species in the disconnected groundwater pond, while mining operations around the cave continue, a modified mining layout

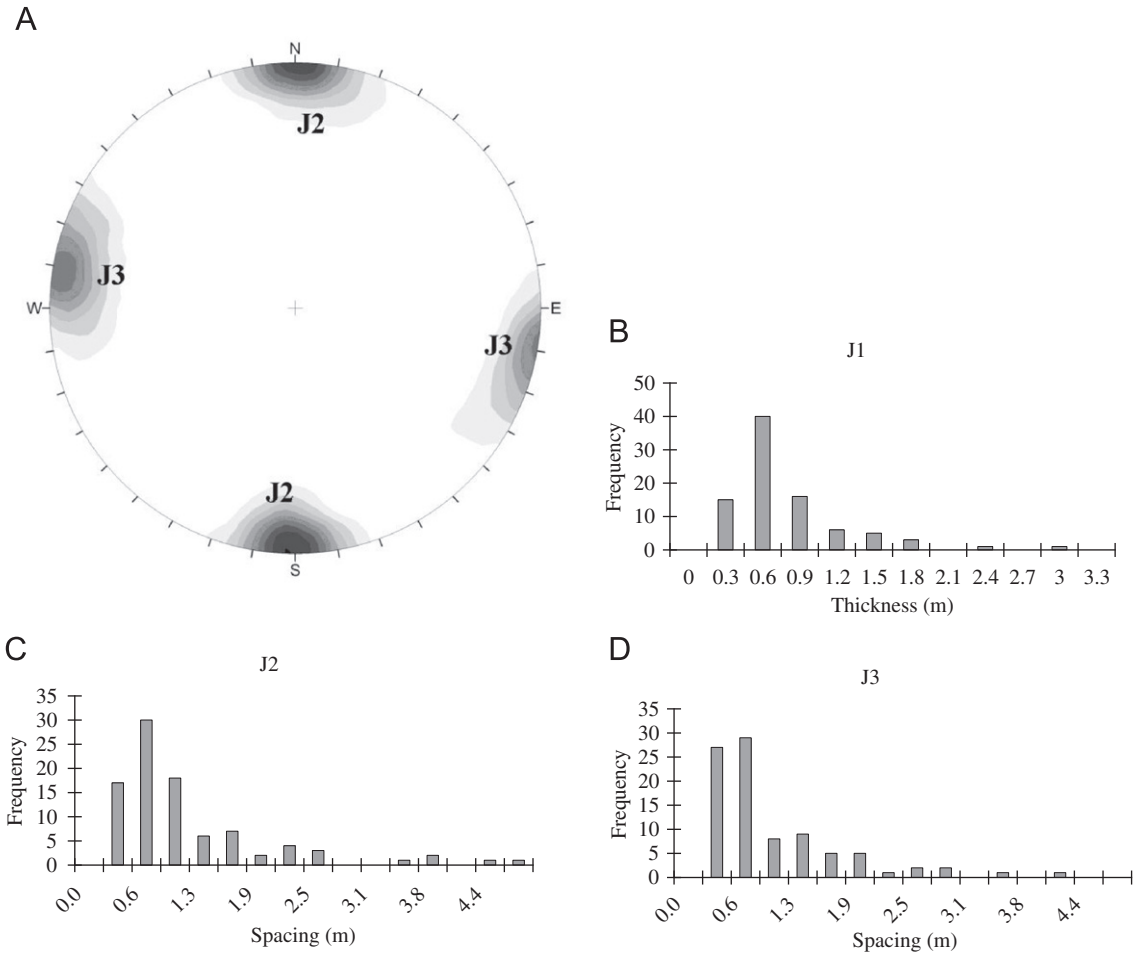

Fig. 11. Rock mass structure at Ramle pit mine: (A) lower hemisphere projection of poles of two vertical joint sets, (B) thickness distribution of bedding planes (J1) that are assumed horizontal, (C) spacing distribution of J2, and (D) spacing distribution of J3.

plan is proposed leaving an elevated trapezoidal structure around the cave, the contours of which are delineated in Fig. 8 in heavy solid line.

To validate our analysis we begin by studying the stability of Ayalon cave under the current geometry of the mine, as the cavern appears to be at least marginally stable since no failure zone has reached the ground surface, till date. A representative cross through Ayalon cave in the current mine geometry (section D–D in Fig. 8) is shown in Fig. 13A. The computed DDA mesh, consisting of 15,011 blocks with a mean block area of 1.07 m^2, is shown in Fig. 13B. The deformation of the block mesh under gravitational load is shown in Fig. 13C for 90,000 time steps representing 35.04 s of real time. The graphical output suggests that, indeed, the opening in the current mine topography is stable. Inspection of the vertical displacement component output in the four measurement points in the roof, however (Fig. 13D), suggests that only half of the roof attains stability with the loosening zone extending to at least half the height of the cover, rendering the structure "marginally stable" according to our classifications in Section 3. Marginal stability can also be inferred from the horizontal stress component outputs recorded in the four measurement points in the roof (Fig. 13E), where only measurement points 1 and 2 in the upper half of the roof attain equilibrium under horizontal (arching) stresses of 400–500 kPa. Note that a significant surface settlement of 1.83 m is expected when the time stable equilibrium is attained (Fig. 13D). These numerical results obtained for the current mine topography are supported by field observations. While the Ayalon cave is free standing, thick sections of the roof have collapsed since the formation of the karstic opening, as can be appreciated from Fig. 9B.

To study the influence of mine layout modification on Ayalon cave after the preservation efforts are complete, we analyze cross-section C–C′ (Fig. 8) but in the final mine topography (Fig. 14A). The modeled block mesh (Fig. 14B) consists of 13,838 individual blocks with mean block area of 1.10 m^2. The deformation of the bock mesh under gravitational load is shown in Fig. 14C for 100,000 computation time steps, equivalent here to 46 s of real time. The performance of the modeled structure can be appreciated by inspection of the vertical displacement and horizontal stress components in the roof as recorded in the four measurement points throughout the analysis (Fig. 14D–E). Surprisingly, cutting the right side of the section thus removing lateral confinement does not alter the stability too drastically, and again "marginal stability" is obtained. As in the previous case the loosening zone extends to half the height of the cover, but the upper half of the roof, as expressed by the outputs of measurement points 1 and 2, attains equilibrium with solid arching stress development at a level of 200–400 kPa. Note that a significant settlement of the surface is expected once equilibrium is reached, of 1.47 m. Analysis of section D–D′ after mine layout modification in the same way provides similar results, with total ground settlement of 2.25 m after equilibrium is attained. The computed response of section D–D′ before and after mine modification, as expressed in vertical deflection of the four measurement points in the roof, is shown in Fig. 15.

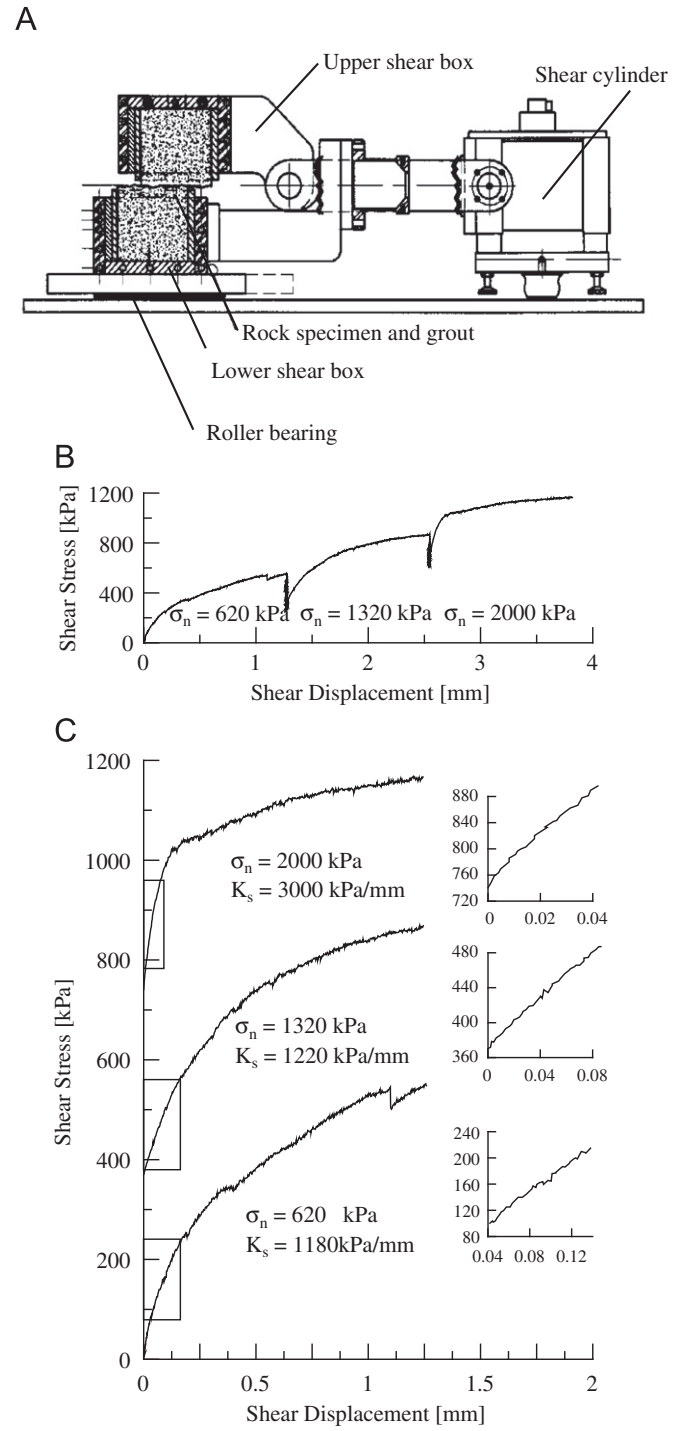

Fig. 12. Direct shear test results for a representative bedding plane interface: (A) shear box assembly, (B) composite plot showing three segments of direct shear, (C) individual shear segments (liner part of the curve used for Ks regression is shown in inset). Direct shear tests were performed under an imposed constant normal stress and at a constant shear displacement rate of 0.027 mm/s.

5. Discussion

Sinkhole collapse in active open pit mines can pose significant safety concerns in routine mining operations. Karstic caverns are difficult to detect with shallow geophysics and therefore mines may have to resort to the more costly alternative of exploration drilling. Optimal and economic dimensioning of the drilling pattern (distance between boreholes and minimum depth of boreholes) must involve basic assumptions regarding the minimum cover height required for stability of a cavern with a given span.

In Section 3 we have delineated a curve in cover height vs. cavern span space (Fig. 7) that marks the boundary between stable and unstable shallow cavern geometries, for blocky rock masses consisting of horizontal to sub-horizontal bedding planes and vertical to sub-vertical joints (for stability of underground openings in discontinuous rock masses containing inclined joints see for example [35]). The boundary between stable and unstable geometries is obtained here using numerical analysis of nineteen different models (see Table 1) with a total number of blocks increasing from 871 in the smallest model (Model 1) to 11,104 in the largest (Model 10). The results suggest that for cavern spans of up to 18 m a shallow cover height of 6 m only ($h/B=0.33$) is sufficient for stability for blocky rock masses modeled here (see geometrical and mechanical parameters in Tables 2 and 3). For spans greater than 18 m the demand for cover height increases very rapidly from $h/B=0.33$ for $B=18$ m to $h/B=1.0$ for $B=26$ m. Beyond $B=26$ m the demand for cover/span ratio seems to remain constant at $h/B=1.0$, suggesting that at least one opening span is required as cover height to ensure stability of shallow caverns in such spans.

To test our numerical modeling results we check the stability boundary obtained by us semi-empirically (Fig. 7), with a shallow, large span, cavern that was explored below an active open pit mine, the Nesher mine near Ramle, Israel. The span of Ayalon cave is 40 m and the current cover height is 30 m only, rendering this structure "marginally stable" based on our stability boundary (see Fig. 7). Indeed both detailed DDA simulations of this structure in the current mine topography (Fig. 13), as well as field observations (Fig. 9B) support this conclusion as the immediate roof layers do collapse, yet the upper half of the roof attains equilibrium under gravitational loads, as proved by zero change in vertical deflection rate and solid arching stress development in the upper two measurement points in the roof, and the pile of blocks assembled on the floor of the cave below the immediate roof.

Another test for our semi-empirical stability boundary for shallow karstic caverns is the case of Zedekiah cave reported by us elsewhere [19]. Zedekiah cave is in fact an old stone quarry below the old city of Jerusalem dated back to the Roman period. The span of the largest chamber in the cave, known locally as the "Freemasons' hall", is 30 m and the height of cover is 25 m. The cave was quarried in a rock mass similar to the case of Ayalon cave but with more widely spaced joints and lower strength level of intact rock elements. Zedekiah cave plots on the boundary between marginally stable and unstable (see Fig. 7). Indeed, although the cave has been free standing for at least 2000 years, some slabs have collapsed from the roof in several chambers (see Fig. 2 in [19]) indicating marginal stability.

Finally, a case of an ancient underground water reservoir at Tel Beer Sheva dated back to the Bronze period was reported by us elsewhere [17], where a free span of 20 m was attempted by the ancient engineers with a cover height of only 5 m in blocky chalk rock mass, with intact rock strength and mean joint spacing much lower than in the two other cases described above. Field evidence indicate that the roof collapsed immediately after the opening has been excavated and the ancient workers constructed a pillar to support the remaining roof against future collapse (see Fig. 5 in [17]), as can be inferred from the same type of plaster used to cover both the room and segment of the collapsed roof side walls (for more details see [17]). Field observations therefore suggest that the attempted geometrical configuration is unsafe, and this is also predicted by our semi-empirical model (Fig. 7).

To conclude the discussion, we have shown using three case studies that our predictive model remains valid even in very different rock masses, as long as the general "blocky" rock mass configuration is maintained. Intact rock strength, rock density, joint

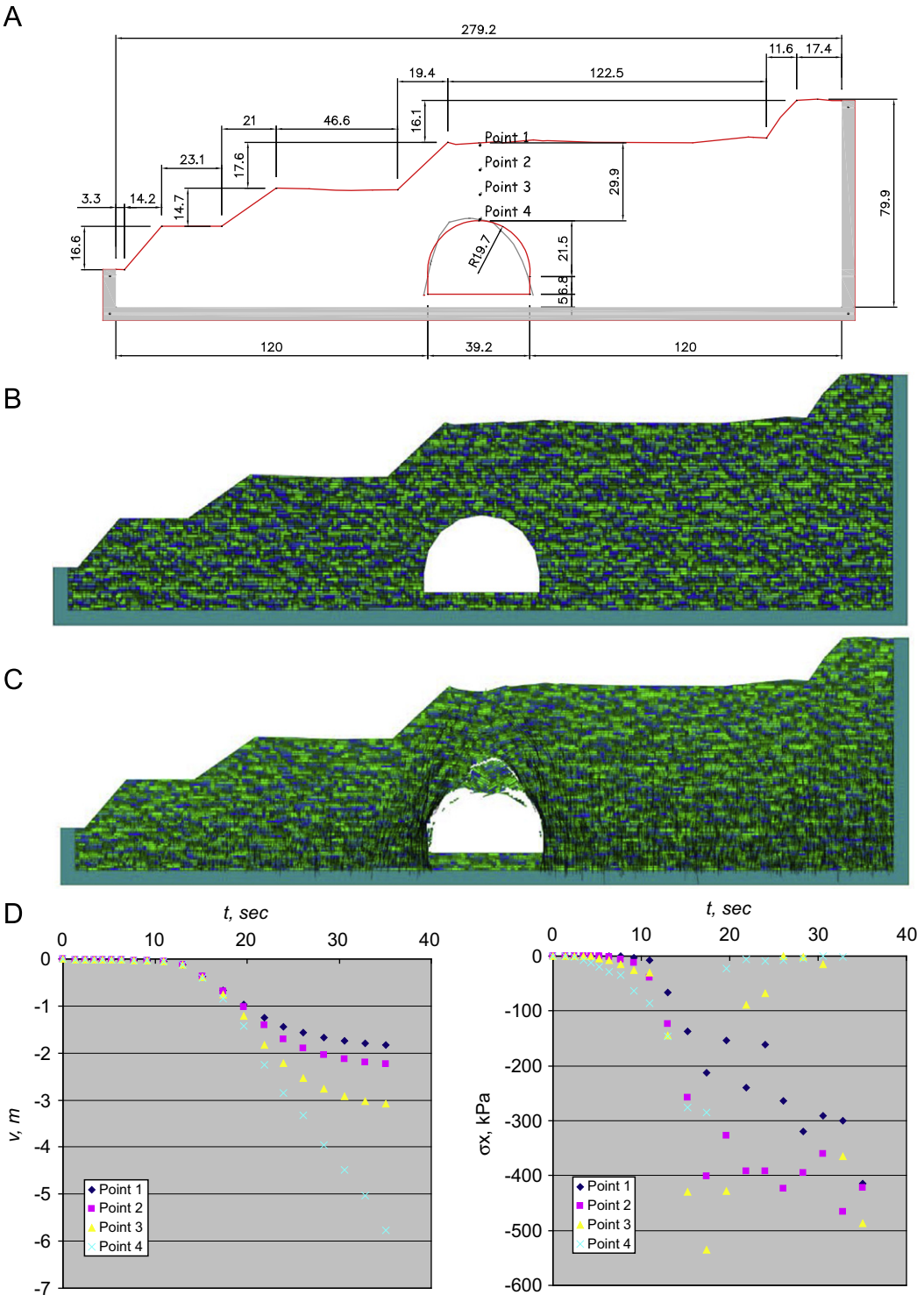

Fig. 13. Ayalon cave in the current mine topography, section D–D′: (A) geometrical parameters, (B) DDA mesh, (C) graphical output of forward DDA computation after 35 s of real time, (D) vertical deflection, and (E) horizontal stress components as recorded in four measurement points in the roof.

friction, and joint spacing may vary between different cases, yet the general shape of the limiting relationship is expected to remain the same, as long as the rock mass structure may be classified as "blocky".

While our numerically obtained stability boundary (Fig. 7) seems to be confirmed by independent field case studies in different blocky rock masses, it must be remembered that the model has several restrictions: (1) It is only valid for blocky rock masses where the bedding planes are horizontal to sub-horizontal and the joints are vertical to sub-vertical. (2) The model was developed for highly fractured rock masses with mean joint spacing in the order of 1 m. Rock masses with wider joint spacing may be expected to be safer. (3) The model was developed for weak to medium strength rocks with UCS of 10–50 MPa. It should not be applied in very weak and soft rock masses even when they apparently exhibit a blocky structure. (4) Our analysis is strictly two dimensional. Typically, a three-dimensional analysis will be less conservative and more realistic. It may therefore be assumed

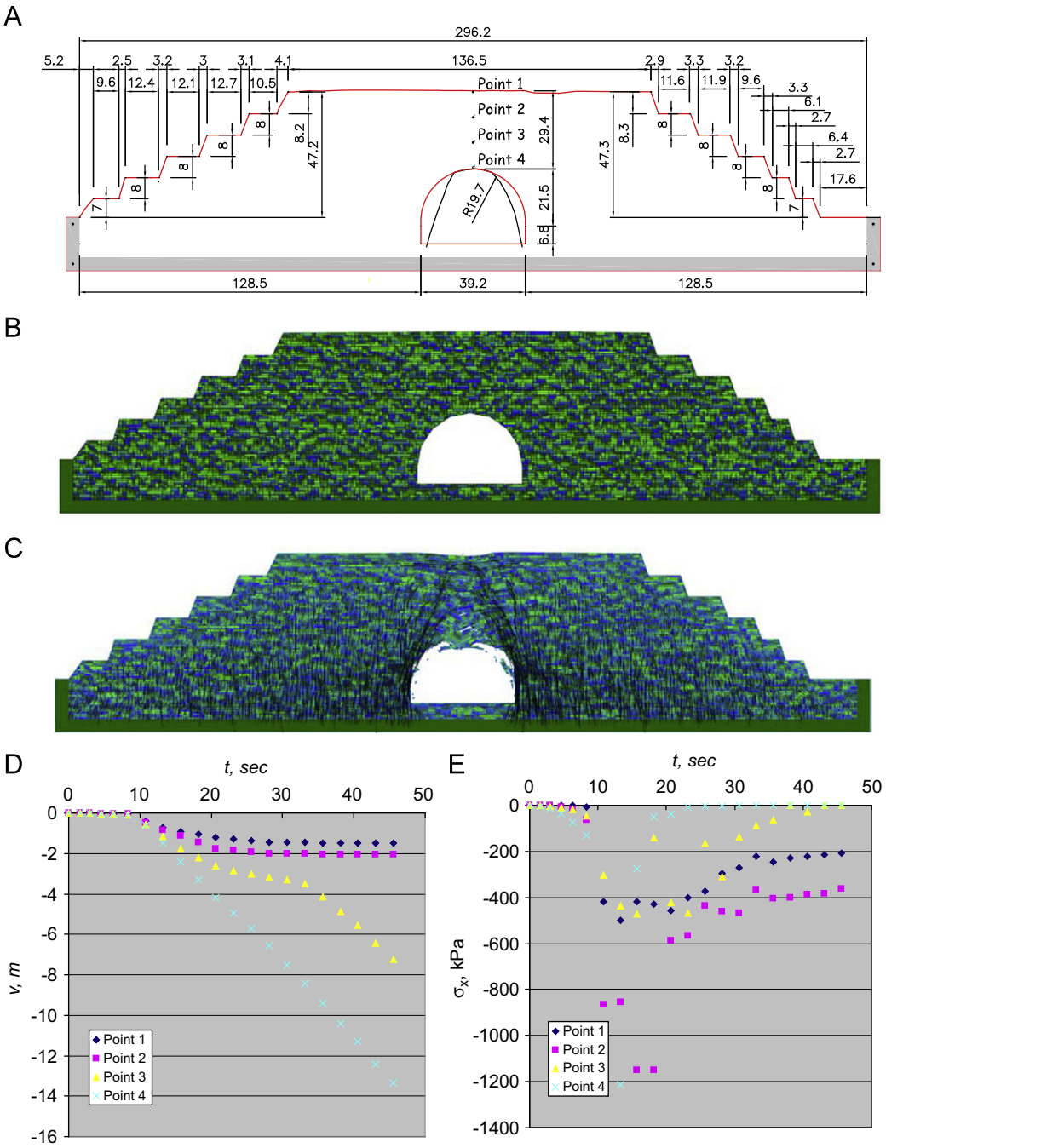

Fig. 14. Ayalon cave in the proposed modified outline of the mine, section C–C′: (A) geometrical parameters, (B) DDA mesh, (C) graphical output of forward DDA computation after 46 s of real time, (D) vertical deflection, and (E) horizontal stress components as recorded in four measurement points in the roof.

that because our analysis is restricted to two dimensions our results are slightly conservative. This can be seen in Fig. 7 with respect to both Ayalon and Zedekiah caves.

6. Summary and conclusions

Sinkhole collapse in active open pit mines can pose significant safety concerns in routine mining operations.

Karstic caverns are difficult to detect with shallow geophysics and therefore mines may have to resort to the more costly exploration drilling alternative. Optimal and economic dimensioning of the drilling pattern (distance between boreholes and minimum depth of boreholes) must involve basic assumptions regarding the minimum cover height required for stability of a cavern with a given span.

We develop here, using the numerical DDA method, a function that marks the boundary between stable and unstable shallow cavern geometries, for blocky rock masses consisting of horizontal to sub-horizontal bedding planes and vertical to sub-vertical joints.

Our results suggest that for cavern spans of up to 18 m a shallow cover height of 6 m only ($h/B=0.33$) is sufficient for stability for the blocky rock mass modeled here. For spans greater than 18 m the demand for cover height increases very rapidly from $h/B=0.33$ for $B=18$ m to $h/B=1.0$ for $B=26$ m. Beyond $B=26$ m the demand for cover/span ratio seems to remain constant at $h/B=1.0$, suggesting that at least one opening span is required as cover height to ensure stability of shallow caverns in such spans.

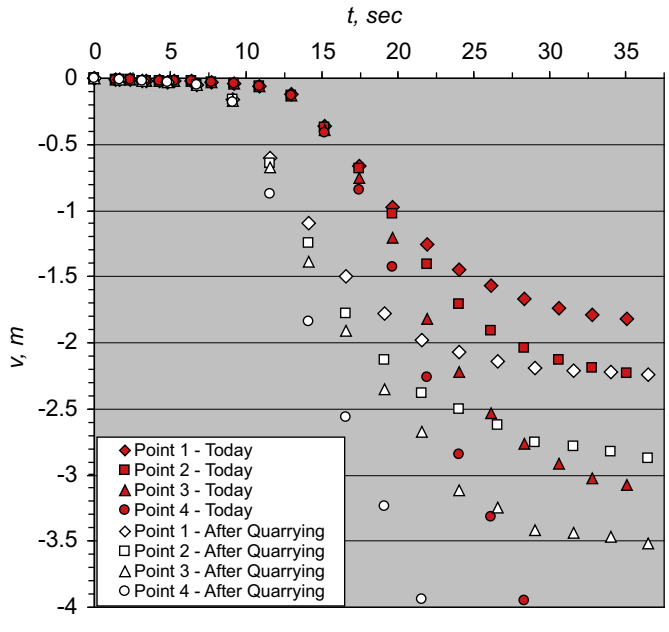

Fig. 15. Response of section D–D′ to mine layout modification (open symbols) in comparison to current condition.

Our results are confirmed by three independent stability analyses of underground openings in blocky rock masses possessing different mechanical properties for intact rock elements as well as different joint friction and spacing.

Acknowledgements

This research was funded by Nesher—Israel Cement Enterprises. Uri Mor and Yoram Golan of Nesher are thanked for their collaboration and for professional discussions, Dr. Y. Mimran of Israel Ministry of Infrastructure and Prof. A. Frumikn of the Hebrew University are thanked for stimulating discussions. Comments received from two anonymous reviewers improved the quality of this paper.

References

[1] Marinos PG. Tunneling and mining in karstic terrain: an engineering challenge. In: Proceedings of the eighth multidisciplinary conference on sinkholes and the engineering and environmental impacts of karsts, Louisville, Kentucky; 2001. p. 3–16.
[2] Milanovic P. Tunneling in karst: common engineering-geology problems. In: Proceedings of the International Symposium of Engineering Geology Environment, Athens; 1997. p. 2797–802.
[3] Milanovic P. Prevention and remediation in karst engineering. In: Proceedings of the ninth multidisciplinary Conference on sinkholes and the engineering and environmental impacts of karsts, Huntsville, Ala; 2003. p. 3–28.
[4] Castillo LV, Molina CR. Geotechnical engineering and geology for a highway through cone karst in Puerto Rico. In: Proceedings of the eighth multidisciplinary conference on sinkholes and the engineering and environmental impacts of karsts, Harrisburg, Penn; 1999. p. 431–45.
[5] Amin AA, Bankher KA. Karst hazard assessment of eastern Saudi Arabia. Nat Hazards 1997;15(1):21–30.
[6] Tharp TM. Design against collapse of karst caverns. In: Proceedings of the fifth multidisciplinary conference on sinkholes and the engineering and environmental impacts of karsts, Gatlinburg, Tenn; 1995. p. 397–406.
[7] Fazeli MA. Construction of grout curtain in karstic environment case study: Salman Farsi Dam. In: Proceedings of the international conference on water resources and environmental problems in karst, Belgrade; 2005. p. 791–96.
[8] Matheson GM, Miller DK, et al. Influence of blasting on sinkhole development near limestone quarries. In: Proceedings of the 24th annual conference explosives and blasting technique, New Orleans; 1998. p. 605–16.
[9] Legchenko A, et al. Locating water-filled karst caverns and estimating their volume using magnetic resonance soundings. Geophysics 2008;73(5):G51–61.
[10] Murphy P, et al. Enhancing understanding of breakdown and collapse in the Yorkshire Dales using ground penetrating radar on cave sediments. In: Proceedings of the first generation Mtg european geosciences union, Nice; 2004. p. 160–8.
[11] Oluic M, et al. Investigation of the landfill location in karst area using RS and geophysical survey—case study Lecevica, Split (Croatia). In: Proceedings of the 24th symposium of the european association remote sensing laboratories (EARSeL), Dubrovnik; 2004. p. 601–7.
[12] Dembicki EA, Mache HG. Recognition and delineation of paleokarst zones by the use of wireline logs in the bitumen-saturated Upper Devonian Grosmont Formation of northeastern Alberta, Canada. AAPG Bull 1996;80(5):695–712.
[13] Ferronato M, Gambolati G, Teatini CJP. Numerical modelling of regional faults in land subsidence prediction above gas/oil reservoirs. Int J Numer Anal Methods Geomech 2008;32(6):633–57.
[14] Jiang YJ, Li B, Yamashita Y. Simulation of cracking near a large underground cavern in a discontinuous rock mass using the expanded distinct element method. Int J Rock Mech Min Sci 2009;46(1):97–106.
[15] Cai M, et al. FLAC/PFC coupled numerical simulation of AE in large-scale underground excavations. Int J Rock Mech Min Sci 2007;44(4):550–64.
[16] Terzaghi K. Load on tunnel supports. In: Proctor RV, White TL, editors. Rock tunneling with steel supports. Ohio: Commercial Shearing Inc.; 1946. p. 47–86.
[17] Hatzor YH, Benary R. The stability of a laminated Voussoir beam: back analysis of a historic roof collapse using DDA. Int J Rock Mech Min Sci 1998;35(2):165–81.
[18] Hatzor YH, Tsesarsky M, Eimermacher RC. Structural stability of historic underground openings in rocks: two case studies from Israel. In: Kouroulis SK, editor. Fracture and failure of natural building stones. Berlin: Springer; 2006. p. 215–37.
[19] Bakun-Mazor D, Hatzor YH, Dershowitz W. Modeling mechanical layering effects on stability of underground openings in jointed sedimentary rocks. Int J Rock Mech Min Sci 2009;46(2):262–71.
[20] Tsesarsky M, Hatzor YH. Tunnel roof deflection in blocky rock masses as a function of joint spacing and friction—a parametric study using discontinuous deformation analysis (DDA). Tunnelling Underground Space Technol 2006;21(1):29–45.
[21] Shi GH, Goodman RE. The key blocks of unrolled joint traces in developed maps of tunnel walls. Int J Numer Anal Methods Geomech 1989;13:131–58.
[22] Hatzor YH, Talesnick M, Tsesarsky M. Continuous and discontinuous stability analysis of the bell-shaped caverns at Bet Guvrin, Israel. Int J Rock Mech Min Sci 2002;39(7):867–86.
[23] Shi GH. Block system modeling by discontinuous deformation analysis. In: Brebbia CA, Connor JJ, editors. Topics in engineering, vol. 11. Southampton: UK: Comp Mech Pub; 1993.
[24] Doolin DM, Sitar N. Time integration in discontinuous deformation analysis. J Eng Mech ASCE 2004;130(3):249–58.
[25] Wang CY, Chuang CC, Sheng J. Time integration theories for the DDA method with finite element meshes. In: Proceedings of the first international forum on discontinuous deformation analysis (DDA) and simulation of discontinuous media, Berkeley; 1996. p. 263–87.
[26] Jing LR. Formulation of discontinuous deformation analysis (DDA)—an implicit discrete element model for block systems. Eng Geol 1998;49(3-4):371–81.
[27] MacLaughlin MM, Doolin DM. Review of validation of the discontinuous deformation analysis (DDA) method. Int J Numer Anal Methods Geomech 2005;30:271–305.
[28] Hatzor YH, et al. Dynamic stability analysis of jointed rock slopes using the DDA method: King Herod's Palace, Masada, Israel. Int J Rock Mech Min Sci 2004;41(5):813–32.
[29] Wu JH, Ohnishi Y, Nishiyama S. A development of the discontinuous deformation analysis for rock fall analysis. Int J Num Anal Meth Geomech 2005;29(10):971–88.
[30] Tsesarsky M, Hatzor YH, Sitar N. Dynamic displacement of a block on an inclined plane: Analytical, experimental and DDA results. Rock Mech Rock Eng 2005;38(2):153–67.
[31] Diederichs MS, Kaiser PK. Stability of large excavations in laminated hard rock masses: the voussoir analogue revisited. Int J Rock Mech Min Sci 1999;36(1):97–117.
[32] Sofianos I. Analysis and design of an underground hard rock Voussoir beam roof. Int J Rock Mech Min Sci 1996;33(2):153–66.
[33] Milstein M. Prehistoric cave discovered: 8 new species thrive inside. Natl Geogr News 2006.
[34] Barton N. The shear strength of rock and rock joints. Int J Rock Mech Min Sci 1976;13:255–79.
[35] Wu JH, Ohnishi Y, Nishiyama S. Simulation of the mechanical behavior of inclined jointed rock masses during tunnel construction using discontinuous deformation analysis (DDA). Int J Rock Mech Min Sci 2004;41(5):731–43.